Naval Research Laboratory

Washington, DC 20375-5320

NRL/FR/5715--95-9759

Comparison of Fiber-Optic and a P-I-N Diode RF Phase Shifter

JAMES L. DEXTER

Optical Physics Branch
Optical Sciences Division

CIARAN J. MURPHY

Off-Board Countermeasures Branch
Tactical Electronic Warfare Division

September 30, 1995

REPORT DOCUMENTATION PAGE

Form Approved
OMB No. 0704-0188

1. AGENCY USE ONLY (*Leave Blank*)	2. REPORT DATE	3. REPORT TYPE AND DATES COVERED
	September 30, 1995	

4. TITLE AND SUBTITLE

Comparison of a Fiber-Optic and a P-I-N Diode RF Phase Shifter

5. FUNDING NUMBERS

6. AUTHOR(S)

James L. Dexter and Ciaran J. Murphy

7. PERFORMING ORGANIZATION NAME(S) AND ADDRESS(ES)

Naval Research Laboratory
Washington, DC 20375-5320

8. PERFORMING ORGANIZATION REPORT NUMBER

NRL/FR/5710--95-9759

9. SPONSORING/MONITORING AGENCY NAME(S) AND ADDRESS(ES)

Office of Naval Research
Arlington, VA 22217

10. SPONSORING/MONITORING AGENCY REPORT NUMBER

11. SUPPLEMENTARY NOTES

12a. DISTRIBUTION/AVAILABILITY STATEMENT

Approved for public release distributon unlimited.

12b. DISTRIBUTION CODE

13. ABSTRACT (*Maximum 200 words*)

The performance of a conventional p-i-n diode microwave phase shifter is directly compared, in this report, to that of a fiber-optic microwave phase shifters. The fiber-optic system is based upon the technique of fiber stretching, which produces a continuous true-time delay in contrast to the discrete nature of the p-i-n diode phase shifter. The proliferation of microwave fiber-optic links has driven the effort to develop fiber-optic equivalents to standard microwave components. Comparisons are made between the two systems bandwidth, maximum phase shift, amplitude stability, phase accuracy, shifting speed, sideband suppression, insertion time delay, insertion loss, size and power consumption.

14. SUBJECT TERMS

15. NUMBER OF PAGES

25

16. PRICE CODE

17. SECURITY CLASSIFICATION OF REPORT	18. SECURITY CLASSIFICATION OF THIS PAGE	19. SECURITY CLASSIFICATION OF ABSTRACT	20. LIMITATION OF ABSTRACT
UNCLASSIFIED	UNCLASSIFIED	UNCLASSIFIED	UL

NSN 7540-01-280-5500

Standard Form 298 (Rev. 2-89)
Prescribed by ANSI Std 239-18
298-102

CONTENTS

COMPARISON OF A FIBER-OPTIC AND A P-I-N DIODE RF PHASE SHIFTER

INTRODUCTION

Radio frequency (RF) phase shifters are used in a wide variety of applications, from beam steering of phased array radars [1] to RF feeds for particle accelerators [2]. This report will examine a p-i-n diode phase shifter and a fiber-optic line stretching phase shifter. The p-i-n diode phase shifter chosen for this report is the General Microwave 7728 that uses the RF vector modulator approach. This device generates a frequency independent 0 to 2π phase shift in a series of N discrete steps. In contrast, the fiber-optic phase shifter produces a continuous true-time delay phase shift by stretching an optical fiber through which a RF modulated light signal is transmitted. The techniques differ in the method of producing a phase shift. But, in this report they are compared because a fiber-optic phase shifter that can operate up to 18 GHz has been developed and has overlapping performance characteristics similar to a p-i-n diode phase shifter. A variety of applications exist where a RF system has an optical channel for RF signal processing. In such a system there may be an option to perform phase modulation in either the RF or optical domain. This report presents measurements of a similar performance's parameters for the General Microwave 7728 and the fiber-optic phase shifter for the purpose of considering either technique. The report also presents the fabrication of the fiber-optic phase shifter and operational issues in detail This study directly compares these two different techniques bandwidth, maximum phase shift, amplitude variation, phase variation, shifting speed, frequency translation, insertion time delay, insertion loss, size, and power consumption. Frequency translation is performed by the technique of serrodyne modulation of the phase shifter. The translation frequency of the measurements, that will also be referred to as serrodyne measurements, are impacted by the phase shifter bandwidth, maximum phase shift, amplitude variation, phase accuracy, and shifting speed. Special attention is devoted to the serrodyning performance.

THEORY

A phase shifting device is capable of producing a frequency translation. This is done by serrodyne modulating the phase shift. In this report, frequency translation is referred to as serrodyning. An ideal serrodyne modulation waveform, as shown in Fig. 1(a) and as the name suggests, is a serrated or sawtooth shaped modulation waveform that generates a repeated linear phase shift. With this, the desired frequency translation is performed with infinitely suppressed sidebands. Any deviation from an ideal serrodyne waveform reduces this suppression, and the strength of the unwanted sidebands can be fully characterized [3-10]. The case that is examined modifies the ideal waveform to include a nonzero flyback time Fig. 1(b). This simulates the actual motion of the piezoelectric actuator in the fiber stretcher. The second nonideal ramp, as shown in Fig. 1(c), is an example of a multistep ramp that simulates the phase shift of a p-i-n diode phase shifter.

Manuscript approved August 7, 1995

Serrodyne Modulation

When the amount of phase shift in the serrodyne waveform is equal to an integral number of wavelengths, a shifted frequency is equal to the original carrier frequency plus the modulation frequency results. If the amount of phase shift is not exactly equal to an integral number of wavelengths, or if the sawtooth waveform has any nonlinear components, or a nonzero flyback time as shown in Fig. 1(b), distortions occur and result in sidebands surrounding the frequency translated carrier that are spaced at multiples of the modulation frequency.

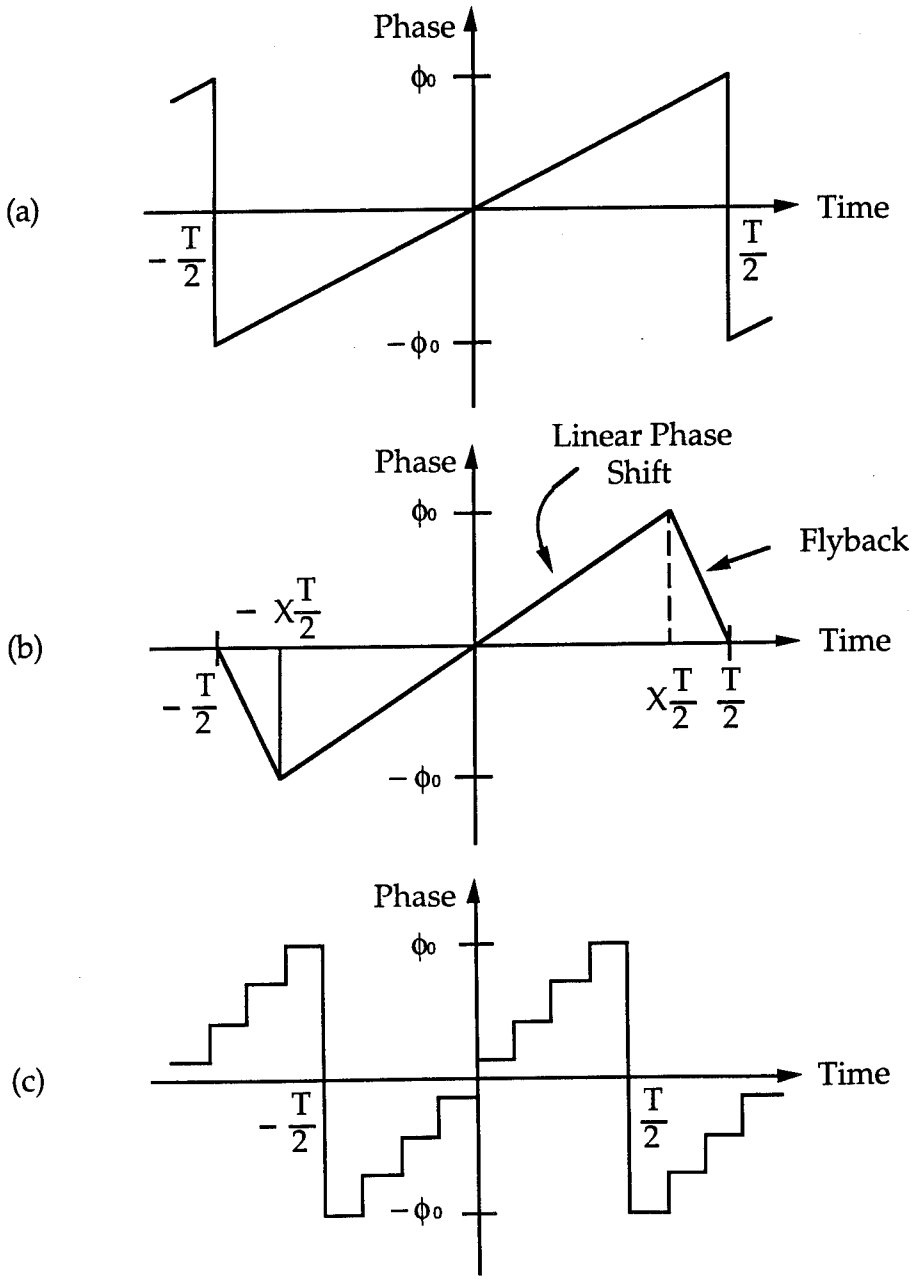

Fig. 1 — Serrodyne modulation waveform. (a) Ideal waveform with continuous linear phase shift and zero flyback, (b) continuous linear phase shift with nonzero flyback, and (c) discrete phase shift eight-step approximation

A phase shifter modulated by the serrodyne waveform produces variations in the phase of the transmitted microwave signal $\phi(t) = \Delta\omega t$ where the equivalent microwave frequency shift is $\Delta\nu = \Delta\omega/2\pi$. The output signal from this microwave phase modulator can be written as

$$\begin{aligned} E_{\text{out}}(t) &= E_0 \exp\{i(\omega_0 t + \phi(t))\} \\ &= E_0 \exp\{i(\omega_0 + \Delta\omega)t\}, \end{aligned} \tag{1}$$

where E_0 and ω_0 are the amplitude and frequency of the input microwave signal. If an ideal sawtooth modulation waveform has an amplitude exactly equal to $m2\pi$, where m is an integer and is equal to the number of 2π phase shifts, the carrier will be completely translated by $\Delta\nu = m/T$ to a new frequency $\omega_0 + m/T$, where T is the sawtooth period. If the sawtooth waveform has any nonlinearity in its ramp or a nonzero flyback time, sidebands will appear. The strength of these sidebands for a nonideal waveform can be determined from the Fourier coefficients of Eq. (1) [6]

$$c_n = \frac{X\sin(\phi_0 - nX\pi)}{\phi_0 - nX\pi} + \frac{(1-X)\sin(\phi_0 - nX\pi)}{\phi_0 - n\pi(X-1)}, \tag{2}$$

where ϕ_0 is the peak phase deviation, Δt is the nonzero flyback period, and $X = (T - \Delta t)/T$. For the case of a ideal sawtooth where $X = 1$

$$c_n = \frac{\sin(\phi_0 - n\pi)}{\phi_0 - n\pi}. \tag{3}$$

If the ideal sawtooth waveform case is examined first, it can be seen that only c_1, the frequency translated carrier with $m = 1$, will be nonzero when $\phi_0 = m\pi$. There are no spurious sidebands. This is true for only a single frequency ω_0 where the fiber has been stretched by an integral number of 2π. At the frequencies surrounding ω_0 the calculated sidebands will grow in strength, Fig. 2. This plot takes into account the frequency dependence of the peak phase variation, with $m = 1$ and $\phi_0 = (\omega/\omega_0)\pi$. The calculated sideband power levels $|c_n|^2$ are plotted as $20\log|c_n|$. This calculation matches with what occurs in a real system. The condition of $2\phi_0 = m2\pi$ is fulfilled for only one frequency, since the maximum fiber stretch is held constant over the whole range of input frequencies. With good carrier suppression over only a small frequency range, serrodyne modulation can only effectively be used in narrowband applications. This small frequency range is diminished further if a higher order of m is used to obtain a larger frequency translation.

The strength of the calculated sidebands is still larger when a nonzero flyback time is included; Fig. 3 was calculated using a 1% flyback time. These calculations were done using a linear ramp. It is assumed that a nonlinear ramp would continue to diminish the relative strength of the frequency translated carrier.

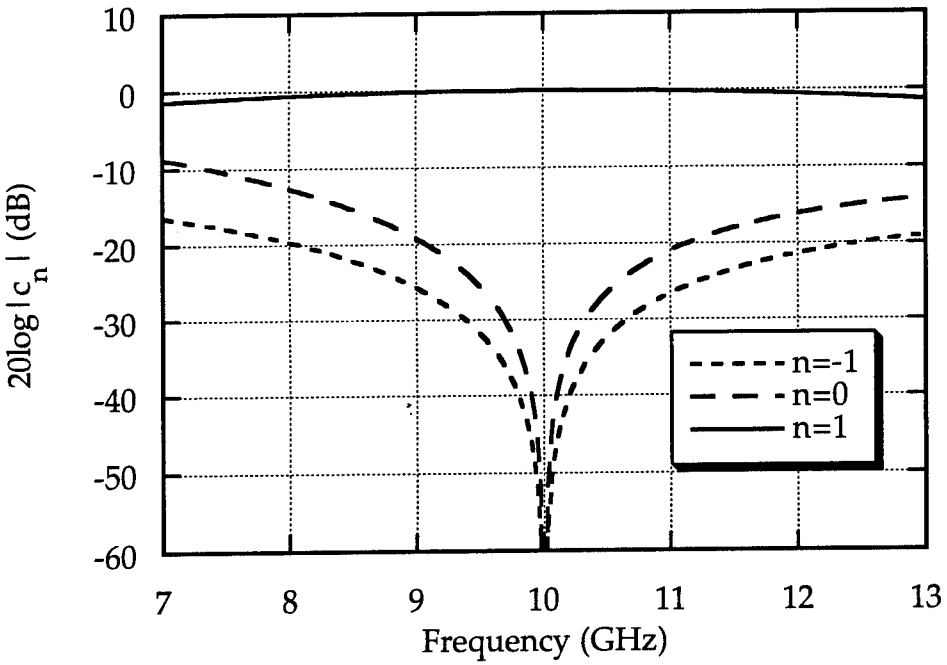

Fig. 2 — Sideband strength with an ideal Serrodyne modulation waveform, $\phi_{0max}=m\cdot\pi$, m=1 at 10 GHz (calculated)

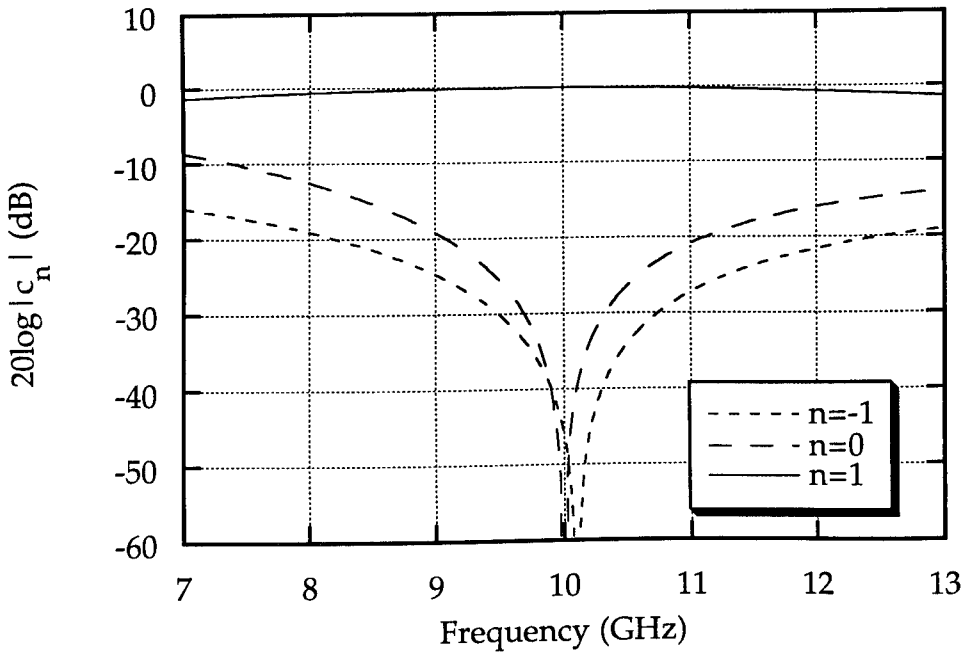

Fig. 3 — Sideband strength with a nonideal, 1% flyback, Serrodyne modulation waveform, m=1 at 10 GHz (calculated)

EXPERIMENTAL PROCEDURES

General Microwave 7728 Phase Shifter

A General Microwave model 7728 phase shifter was used in this comparison. The unit is an 8-bit digital phase shifter with full 360° range. The 8-bit control steps the phase shifter through 256 uniformly spaced phase settings, as the digital input is incremented from 00 Hex to FF Hex the phase shifter increments –1.41° from 0° to –358.6°. Incrementing the 8-bit control form FF Hex to 00 Hex resets the phase shifter back to 0° that is equivalent to 360° of phase shift. This phase shifter operates by separating and recombining the I and Q components of the RF signal. Figures 4 and 5 show the block diagram.

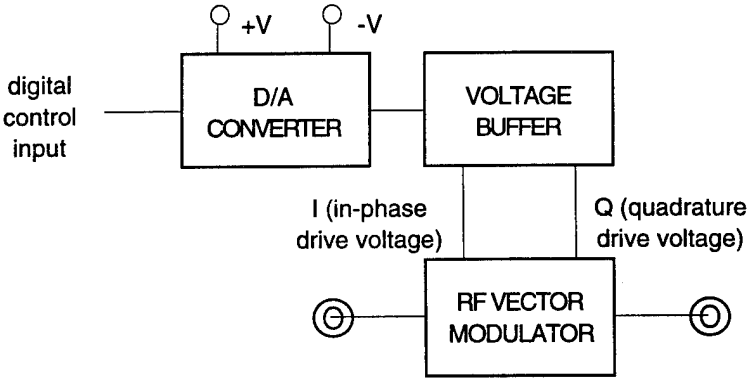

Fig. 4 — Block diagram of the General Microwave model 7728 phase shifter

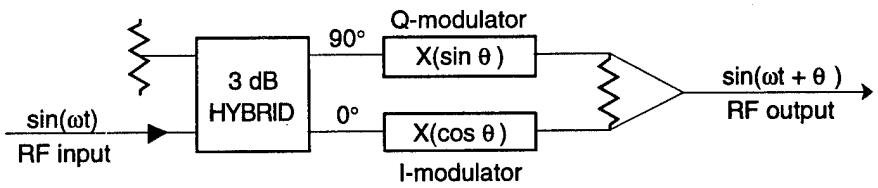

Fig. 5 — Block diagram of a RF vector modulator

Piezoelectric Fiber Stretching Phase Shifter

The fiber-optic phase shifter operates by physically stretching the optical fiber in a microwave fiber-optic link. Figure 6 shows the fiber-optic link. The laser diode is a Lasertron model QLM3S900-005 with a modulation bandwidth of 18 GHz; its 1.3 μm output is coupled into a single-mode fiber. This output fiber is in turn spliced to a length of fiber that is wound around a mount so that an actuator may act upon it to stretch its length. The light is demodulated by using a high-peed photodiode, BT&D/HP model PDC4310-30.

Figure 6 shows the profile of the fiber stretcher mount. The central component is a piezoelectric actuator, Physik Instrumente model P-245.77. The specifications for this preloaded actuator are: maximum pushing force, 1000 N; maximum expansion, 120 μm; stiffness, 8 N/μm; electrical capacitance, 450 nF; diameter, 18 mm; and length, 124 mm [11]. With half shells mounted using set screws to either end of the actuator, optical fiber can now be wound around this structure. This results in an oblong spool of fiber that can have the length of its long axis varied. These half shells are 1.0 in. in diameter and 1.125 in. deep. The dimensions of the constructed fiber stretcher is 5.48 × 1.0 × 1.125 in.

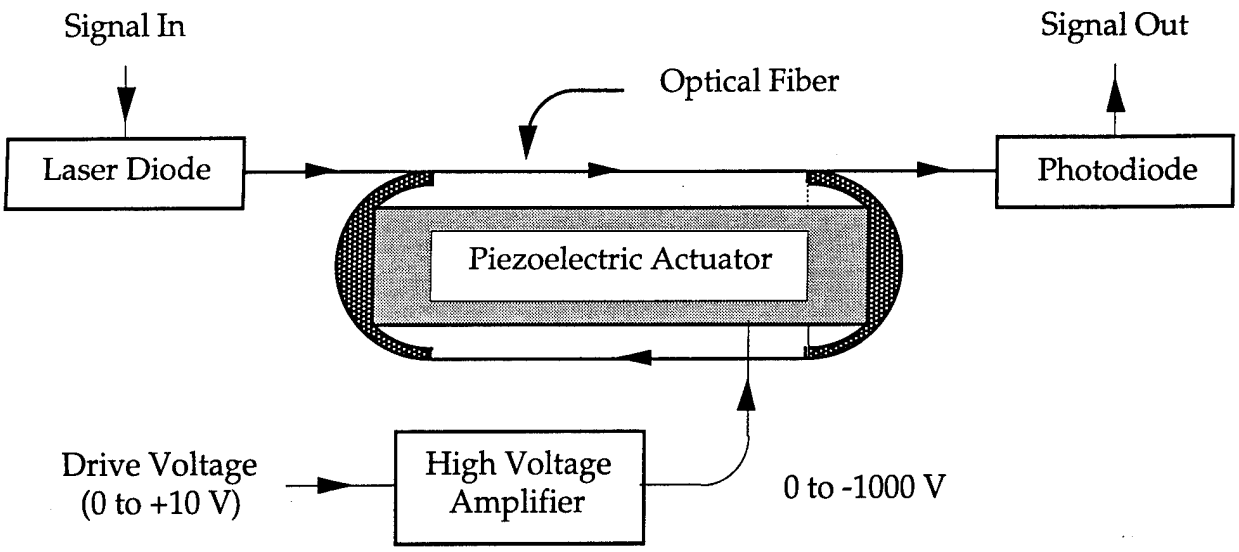

Fig. 6 — Fiber-optic microwave phase shifter. The optical fiber within a fiber-optic link is wound around a mount containing a piezoelectric actuator that is used to stretch the fiber

Standard Corning single-mode telecommunication grade fiber is used, the two standard cladding diameters are 80 and 125 μm. The preferred is the 80 μm fiber because of its higher packing density and the minimization of the required total stretching force. The 80 μm diameter fiber has a coating diameter of 135 μm, which allowed for 187 turns of fiber to be wound onto the oblong spool in a single layer. The length of this fiber, including pigtails, is ~60 m and introduces an insertion delay of ~300 ns. With a maximum allowable expansion of 120 μm, the physical length of the fiber can be stretched by a maximum of

$$\Delta x_{\text{physical}} = (2)(187)(120\ \mu\text{m}) = 4.49\ \text{cm}. \tag{4}$$

The optical path length can therefore vary by,

$$\Delta x_{\text{optical}} = (1.197)\Delta x_{\text{physical}} = 5.37\ \text{cm}, \tag{5}$$

or a calculated maximum phase change of 387° at 6 GHz.

From an electrical standpoint, the piezoelectric actuator can be viewed as a capacitor with a capacitance of 450 *nF* and a maximum drive voltage of 1000 V. To drive this capacitor, a high-voltage amplifier (Physik Instrumente model P-270.01) is used. The amplifier specifications are: maximum output voltage, −1000 V; control voltage, 0 to +10 V; average output current, 0.1 A; peak output current (5 ms), 0.5 A; small signal bandwidth, 5 kHz (500 nF); and large signal bandwidth, 700 Hz. With the above information, the maximum undistorted drive frequency for a triangle wave ν_{max} and the shortest expansion time t_{min} possible can be calculated.

$$n_{\max} = \frac{I_{\max}}{2CV_0} \qquad t_{\min} = \frac{CV_0}{I_{\max}}. \tag{6}$$

In the equations for v_{max} and t_{min}, C is the piezoelectric actuators capacitance 450 nF, and V_0 is taken to be the maximum applicable voltage of 1000 V. To calculate v_{max}, the current I_{max} is set equal to the maximum average current the high voltage amplifier can supply. With I_{max}(average) = 0.1 A, the maximum undistorted drive frequency is 110 Hz. To find t_{min}, I_{max} is set equal to the peak output current for the amplifier, with I_{max}(peak) = 0.5 A the minimum time to full expansion is 0.9 ms. This corresponds well with the measured transition time of 1.0 ms.

When the drive voltage is modulated, the inherent hysteresis and nonlinearity of the piezo can be seen in the fiber stretch. Typically, piezoelectric material has a hysteresis of 10 to 15% and a nonlinearity of 2% [11-13]. When the actuator was modulated by a triangle wave, this hysteresis was evident and was measured to be 10 to 12.7%, depending on the amplitude of the modulation voltage. The expansion of the actuator can be measured vs the applied control voltage by using a displacement transducer installed within the actuator. This hysteresis can be minimized by using a feedback circuit [13,14]; however, such a feedback circuit was not used for these studies. The actuator for the piezoelectric fiber stretcher used a piezostrictive material, a lead zirconate titanate (PZT) based ceramic. Recent experimental work in the manufacturing process of PZT [15] has produced samples with hysteresis of 1.1% and nonlinearity of 0.7%. This technology is still too new to be used in commercially available actuators.

An artifact using piezoelectric actuators is that, after it has been set to a new position, with time the expansion drifts. The drift, which is slow and in the same direction as the movement, is caused by the follow-up polarization of the ceramics. An estimate of the drift that decreases logarithmically with time is [11]

$$\Delta L(t) = \Delta L\left(1 + \gamma \log \frac{t}{0.1}\right), \tag{7}$$

where ΔL is the initial expansion, t is the time after the expansion, and γ is a drift factor that depends on the actuator and the load, typical values are 0.01 to 0.02. This normally small effect is amplified by a factor of 2N because of the fiber stretcher configuration; however, it can be minimized by using a feedback circuit [13,14].

Optical Fiber Kinematics

The mechanics behind the operation of an optical fiber stretcher need to be considered to determine the total force needed to stretch the optical fiber. This information is needed to specify the actuator to be used in the fiber stretcher. An optical fiber will behave as a spring if it is stretched within its elastic limit of <10 to 15%. The spring constant of the optical fiber can be found by using $k = AY/l_0$, where k is the spring constant, A is the cross sectional area of the fiber, Y is the Young's modulus for the fiber, and l_0 is the length of the fiber. The optical fiber is a composite of several materials. The concentric core and cladding are primarily fused silica doped with small percentages of B_2O_3 and GeO_2. They in turn are surrounded by a protective coating of UV curable resin.

The simplest fiber model has three regions: core, cladding, and coating, acting as three springs in parallel. The combined spring constant of N springs, k_1, ..., k_N, in parallel is equal to the sum of the individual spring constants, $k_{total} = k_1 + ... + k_N$. For the case of the optical fiber $k_{total} = k_{core} + k_{cladding} + k_{coating}$. The fibers codopants affects its Young's modulus, but as an estimate the core and cladding

can be taken to be 100% SiO_2, $Y = 7.245 \times 10^{10}\ N/m^2$ [16,17]. Several UV curable resins are used for coating fibers. Their Young's moduli typically fall in the range of $(1.2\text{-}3.7) \times 10^6\ N/m^2$ [18].

The contribution of the coating can be ignored because, even though the core/cladding and coating have comparable cross sectional areas, the coatings Young's modulus is four orders of magnitude smaller than that for the core/cladding combination. As an example, a typical single mode fiber (SMF) that has a 8 μm diameter core of 100% SiO_2, a 125 μm diameter doped cladding, and is coated to a diameter of 250 μm with a UV curable resin will be approximated by a 125 μm diameter fiber of 100% SiO_2.

Once the spring constant is known, the force needed to stretch the optical fiber is determined by Hooke's law, $F = -k_{\text{fiber}}\Delta x_{\text{physical}}$, where k_{fiber} is the fibers spring constant and $\Delta x_{\text{physical}}$ is the elongation, or compression of the spring. The fiber stretcher that will be described below takes the form of two half cylinders that are separated from each other and that are in the same plane. The fiber is then wound around the long axis of this arrangement. The fiber is stretched by changing the separation of these two cylinders, this causes a single loop of fiber to behave as if it were two separate springs in parallel. As stated above, the total spring constant of springs acting in parallel is the sum of the individual spring constants. Therefore the total force required to stretch N loops of fiber is $2N$ times the force needed for a single half loop

$$\begin{aligned} F_{\text{total}} &= 2Nk_{\text{fiber}}\Delta x_{\text{physical}} = 2N\frac{AY}{l_0}\Delta x_{\text{physical}} \\ &= \frac{L_T AY}{l_0^2}\Delta x_{\text{physical}}. \end{aligned} \tag{8}$$

Here k_{fiber} is the spring constant of the fiber when l_0 is taken to be half the fiber loop length, $\Delta x_{\text{physical}}$ is the amount of elongation of l_0, and the total length of the fiber wound on the stretcher is $L_T = 2Nl_0$. Although the force increases linearly with the number of loops, it has a nonlinear dependence with the cylinder separation. Equation (8) shows that the trade-off for making the stretcher small is a requirement for a larger stretching force.

Under normal conditions the optical path length of the fiber is proportional to its physical length, $x_{\text{optical}}=nx_{\text{physical}}$. Because of the fiber stress resulting from stretching the fiber, the photoelastic effect must be taken into account. This effect quantifies the change in the fibers index of refraction due to stress.

A linear index variation of -2.4×10^{-5}/kpsi (-2.7×10^{-3}/% strain) has been measured for both unshifted and dispersion-shifted fiber [19]. The negative slope means that the photoelastic effect has a negative contribution to the fibers optical path length as the fiber is stretched. From this measurement the photoelastic constant can be calculated for standard single-mode fiber

$$\Delta n \equiv -\frac{n^3 p}{2} s$$

so

$$p = \frac{2(\Delta n / s)}{n^3} = \frac{2(0.27)}{(1.4675)^3} = 0.171 \tag{9}$$

where Δn is the index change, p is the photoelastic constant, n is the index of refraction for unshifted fiber (n = 1.4675) [19], and s is the strain. The optical elongation is now

$$\begin{aligned}\Delta x_{\text{optical}} &= n_f L_f - n_i L_i \\ &= (n_i + \Delta n)(L_i + \Delta x_{\text{physical}}) - n_i L_i \\ &= n_i \Delta x_{\text{physical}} + \Delta n(L_i + \Delta x_{\text{physical}}) \\ &= n_i \Delta x_{\text{physical}} - \frac{n_i^3 p}{2} \frac{\Delta x_{\text{physical}}}{L_i}(L_i + \Delta x_{\text{physical}}) \\ &\approx \left(n_i - \frac{n_i^3 p}{2}\right) \Delta x_{\text{physical}} \quad \text{with} \quad L_i >> \Delta x_{\text{physical}}.\end{aligned} \tag{10}$$

The fibers initial unstressed and final stressed indexes of refraction are n_i and n_f, respectively. The fibers initial unstretched length is L_i. After it is stretched by an amount $\Delta x_{\text{physical}}$ its final length is L_f, so that $L_f = L_i + \Delta x_{\text{physical}}$. With Eq. (10) it is possible to calculate the change in the optical path length as a function of how the physical length of the fiber changes. The final approximation in Eq. (10) is valid for piezoelectric actuators because the maximum length variation possible with this type of actuator is only 10^{-3} to 10^{-4}.

Phase Shifter Comparison

To simplify the phase shifter comparison, Table 1 presents the specifications for each. The listed specifications for the General Microwave model 7728 phase shifter are those supplied by the manufacturer. The details of the fiber-optic phase shifter data are mostly contained in the next section.

TEST RESULTS—PERFORMANCE SUMMARY

In this section, the two phase shifters are compared. This is accomplished by measuring the two devices phase shifting capabilities, and the effect they have on the throughput signal amplitude.

Phase vs Frequency and Phase Setting

The fiber-optic phase shifter was configured with a microwave modulated laser and a detector to measure the phase shift across the 6 to 18 GHz band. By setting the voltage for the piezoelectric actuator, the mechanical stretching of the fiber was controlled to produce a true-time delay of the optical channel. The fiber-optic phase shifter was designed to produce at least a 2π phase shift at 6 GHz. To perform this, the piezoelectric actuator needs approximately a 0 to 1000 V high-impedance drive. Figure 7 shows a plot of the phase measurement data. The procedure was to calibrate 0° phase shift to 0/V drive. The drive voltage was then stepped up to create a negative phase shift. The change of phase with voltage over the 6 to 18 GHz band is plotted in Fig. 7. The important characteristic is that the phase change is linear with the frequency. This demonstrates that this technique does generate a true-time delay. Figure 8 shows the second set of data. The nonlinearity observed here is due to the inherent nonlinearity of the piezoelectric actuator, as discussed above. Again the nonlinearity can be minimized by using a feedback circuit. Besides the nonlinearity, phase noise can also be seen in this signal. The standard deviation of this phase noise is 0.88°, 0.85°, 1.72°, 2.21°, and 7.28° at 6, 9, 12, 15 and 18 GHz, respectively. Each component in the fiber-optic link, laser diode,

Table 1 — Comparison of the General Microwave Model 7728 p-i-n Diode and The Fiber-Optic Phase Shifters.

Parameters	General Microwave model 7728	Fiber-optic
Frequency	8-18 GHz (main band) 6-18 GHz (stretch band)	DC-18 GHz
VSWR	2:1	not applicable
Insertion Loss	10 dB	<0.5 dB*
Amplitude Variation	±0.75 dB (main band) ±1.5 dB (stretch band)	±0.05 dB
Phase Shift (maximum)	360° (frequency independent)	408° at 6 GHz (true-time delay)
Phase Accuracy	±12° (main band)	<2.9°
Switching Speed	500 ns	1.0 ms†
Insertion Time Delay	600 ps	300 ns
Power Consumption	+5 V at 250 mA +12 to +15 V at 50 mA −2 to −15 V at 35 mA ≈ 2.5W	45 W‡
Weight	0.113 kg	0.355 kg
Dimensions	0.875 × 2.5 × 3.0 in.	5.48 × 1.0 × 1.125 in.

* Including only the 80/125 μm splice loss.
† With a high voltage amplifier peak current of 0.5 A.
‡ Power consumption for maximum expansion at f = 100 Hz, $P = CV^2f$.

fiber, photodiode and microwave amplifier contributes to this phase noise. That the magnitude of the phase noise increases linearly with frequency, not including the discontinuous jump 18 GHz, suggests that the source is mainly the fiber. With the fiber wrapped around the actuator any variation in the mounts length would be amplified by 2,187. The 0.88° standard deviation at 6 GHz therefore corresponds to a 0.22 μm standard deviation in the length of the mount.

As seen in Figs. 7 and 8, the fiber-optic phase shifter can produce a shift greater than one wavelength at 6 GHz, approximately 408°. This compares well with the predicted phase shift of 387° at 6 GHz.

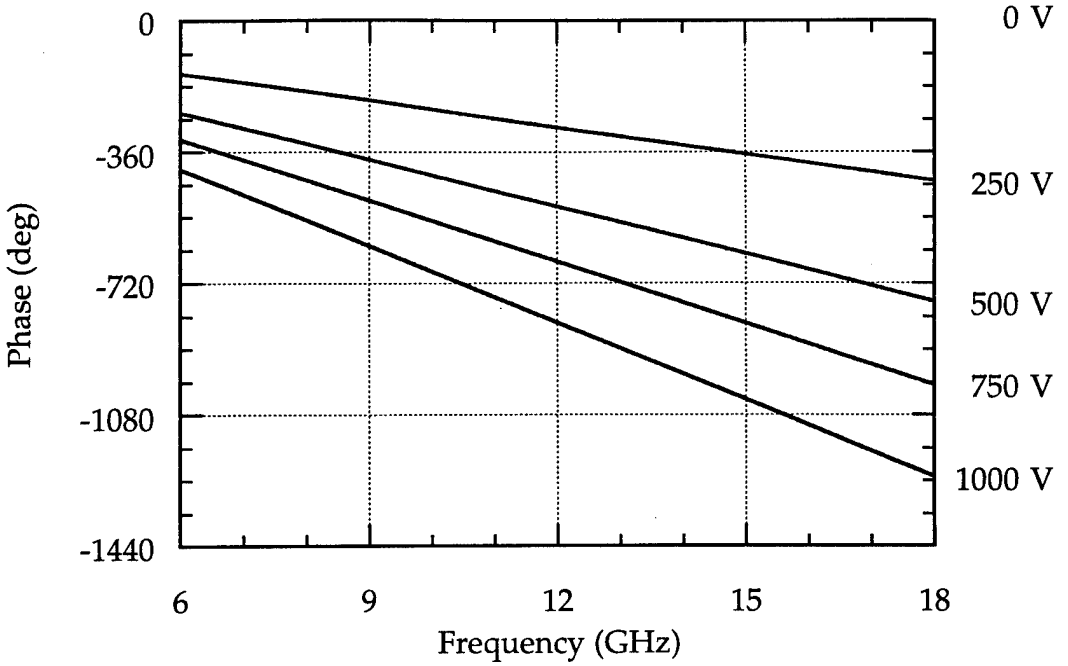

Fig. 7 — Microwave phase shift vs frequency for the fiber-optic phase shifter at several applied voltages (measured)

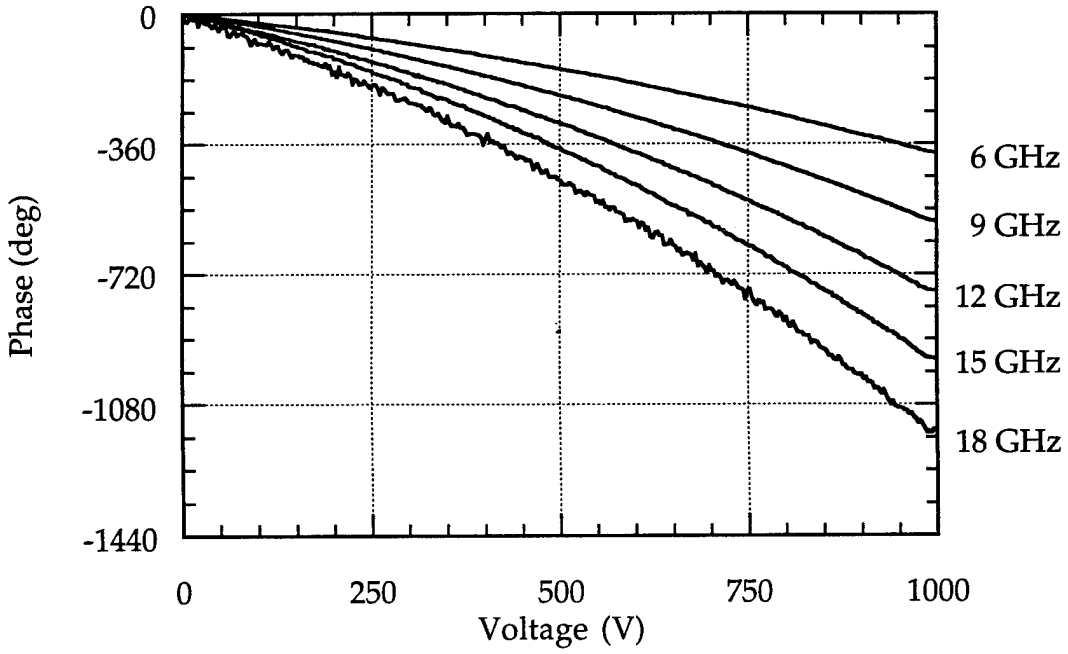

Fig. 8 — Microwave phase shift as a function of the applied voltage for several frequencies, demonstrates the actuators nonlinearity (measured)

The General Microwave 7728 has an 8-bit TTL input to set the phase. The following data, as shown in Fig. 9, are based upon calibrating TTL input of 00 Hex as 0° phase setting. As the digital input is increased, a negative phase shift occurs. The significant characteristic of the data is the constant phase shift vs frequency. This is by design for a p-i-n phase shifter. The data also show the deviation of measured phase vs phase setting, ±12°.

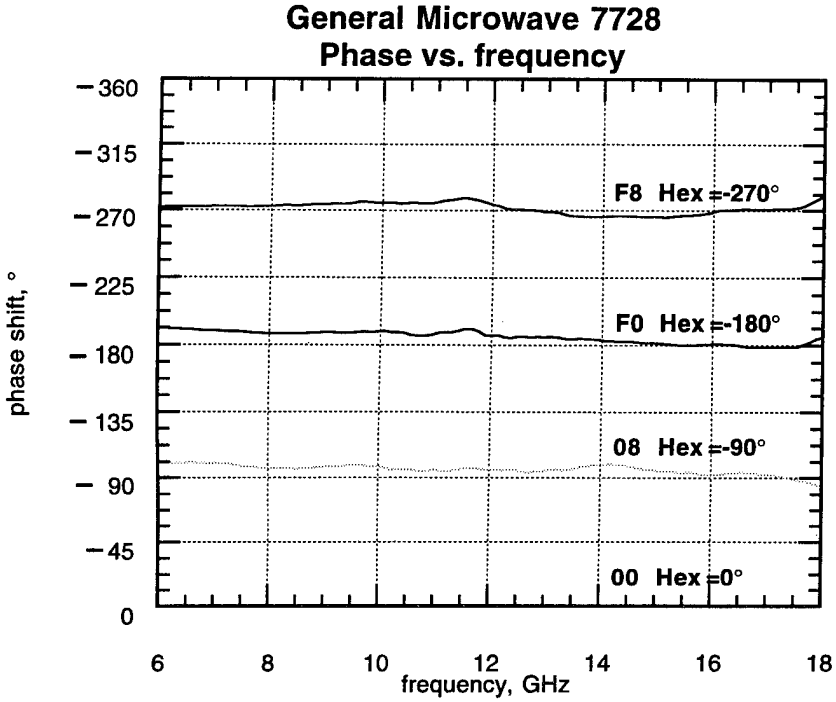

Fig. 9 — Phase variation as a function of frequency for the General Microwave model 7728 phase shifter (measured)

Amplitude vs Frequency and Phase Setting

Figure 10 shows the variation in the throughput signal amplitude was measured for the fiber-optic phase shifter as a function of the applied voltage. This plot does not include the fiber-optic link loss, which is typically 40 to 50 dB. This is justified, because a fiber-optic phase shifter would only be incorporated into a system that already contains a fiber-optic link. Only the variation in the throughput signal amplitude, which is approximately ±0.05 dB, is plotted. These data fall within the measurement error, so effectively there is no variation in amplitude with phase setting. The data for this report are intentionally plotted by using the same scale as the one used for the data of the General Microwave model 7728 phase shifter to emphasize the small amplitude variation as shown in Fig. 11. The fiber-optic phase shifter has a frequency dependent phase shift, therefore an amplitude vs phase setting plot, such as Fig. 11 shows, cannot be generated.

The throughput signal amplitude variation for the General Microwave phase shifter was measured for several frequencies across the 360° phase settings. Figure 11 was generated by incrementing the 8-bit TTL logic and recording the S_{21} magnitude in dB. The plot shows the data for 6, 12, and 18 GHz. The average transfer for the phase shifter is −10 dB, the amplitude varied with phase setting by ±0.75 dB at midband and by ±1.5 dB at the band edges. The important characteristic is that the amplitude is dependent on phase setting, so any phase modulation performed with this device will produce an undesired amplitude modulation.

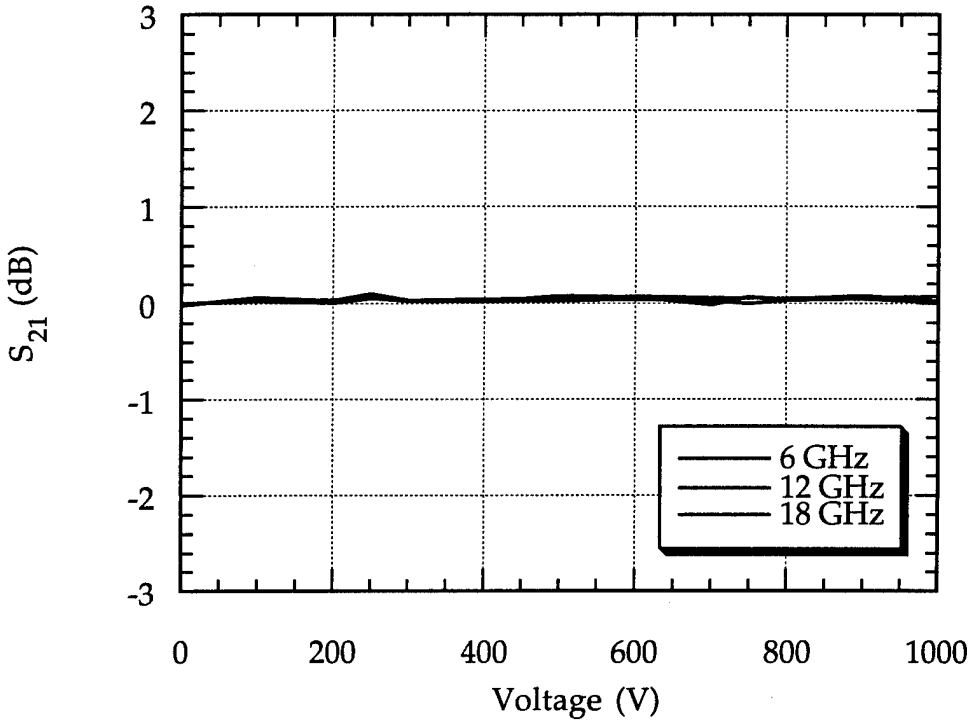

Fig. 10 — Signal amplitude variation vs applied voltage for the fiber-optic phase shifter (measured). The amplitude variation is only ±0.05 dB and is plotted by using the same scale as the one used for the General Microwave model 7728 phase shifter

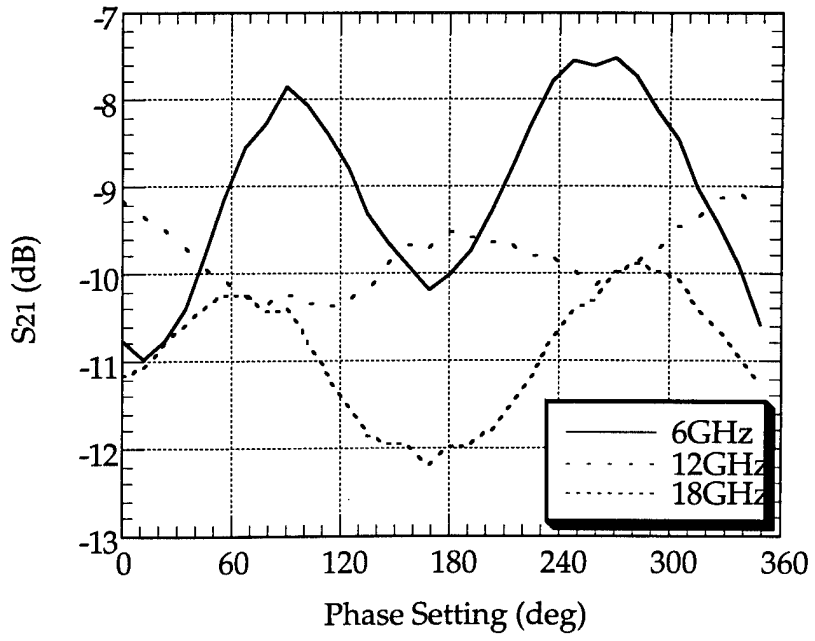

Fig. 11 — Throughput signal amplitude showing the variation with phase setting for the General Microwave Model 7728 phase shifter (measured)

Frequency Translation

A microwave signal will be frequency translated if its phase is serrodyne modulated. The frequency translated spectrums generated by modulating the fiber-optic phase shifter and the General Microwave model 7728 are presented below. These data are presented last, because the performance of the frequency translation by serrodyning is dependent upon several parameters, which include bandwidth, maximum phase shift, amplitude variation, phase accuracy, and shifting speed. For the fiber-optic phase shifter, the serrodyne waveform had a ramp with a positive slope; this simulates the case where the distance between a transmitter and receiver constantly increases. Doing this causes the signal to undergo a negative Doppler shift. The magnitude of the frequency shift depends on the modulation frequency and the amount of phase shift. An input frequency of 12 GHz was used with modulation frequencies of 25, 50, and 100 Hz. The maximum phase shifts were set to 2π and 4π at this input frequency. The frequency spectrums are plotted as the frequency offset from this input carrier frequency. As a reference, Fig. 12 shows an unmodulated spectrum to illustrate the bandwidth and background level of the input microwave signal; the center frequency is 12 GHz.

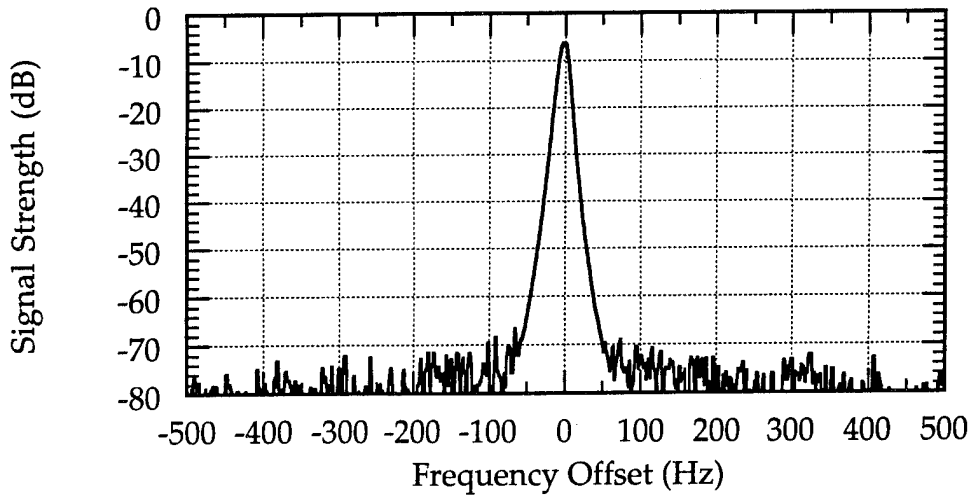

Fig. 12 — Microwave spectrum analyzer output demonstrating the microwave signals unmodulated bandwidth at 12 GHz (measured)

Figure 13 shows the frequency shifted spectrums measured for the General Microwave model 7728 phase shifter. The serrodyne waveform is set for a 2π, m=1, phase shift at 12 GHz, so the calculated carrier frequency shift $\Delta\nu=m/T=1/T$ should be equal to the modulation frequency. Figures 13 (a-c) had modulation frequencies of 25, 50, and 100 Hz respectively, and in each of these figures sidebands were observed with these frequency spacing. The largest sideband in each of these figures is the first sideband in the negative frequency direction n=-1 from the center frequency. The carrier and all other sidebands are suppressed by >25 dB for each of the modulation frequencies; this corresponds to the specifications supplied by the company.

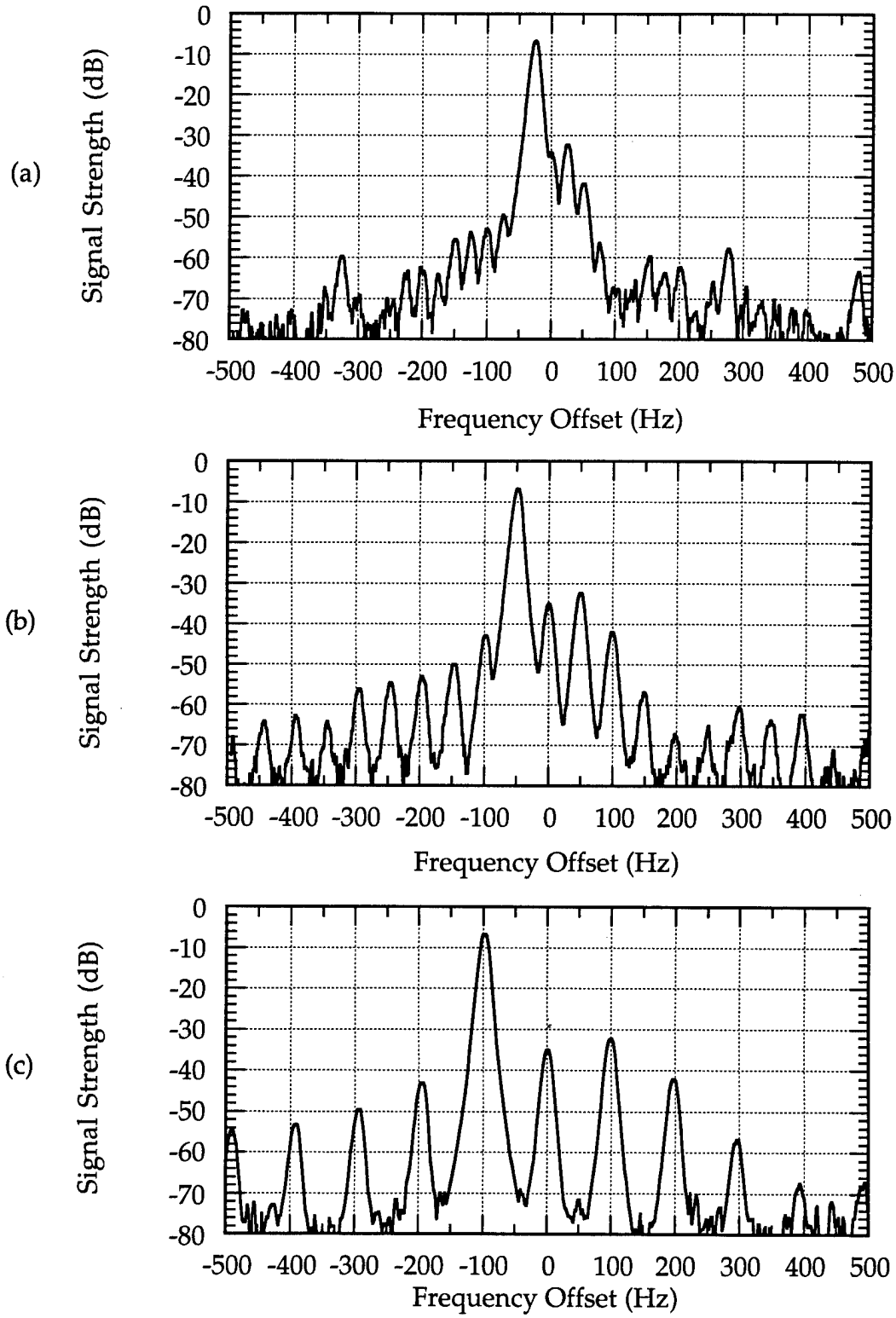

Fig. 13 — Microwave spectrum analyzer output demonstrating the frequency shift generated by the General Microwave model 7728 phase shifter at 12 GHz with a 2π serrodyne modulation at, (a) 25 Hz, (b) 50 Hz, and (c) 100 Hz (measured)

The fiber-optic phase shifter was at first modulated with a serrodyne waveform that matched the settings used with the p-i-n diode phase shifter. The resulting spectrums, shown in Fig. 14 (a-c), have sidebands spaced at intervals equal to the plots corresponding modulation frequency. Again, the largest sideband in each of these cases is the first negative sideband n=-1 just as predicted. From these plots, the suppression of the sidebands is seen to decrease as the modulation frequency increases. The measured carrier suppression at 25, 50 and 100 Hz is >23, >22 and >18 dB, respectively. This decrease in suppression is predicted by Eq. (2). If Δt is fixed, the predicted strength of the unwanted sidebands increases as the modulation frequency increases. The factor $X=(T-\Delta t)/T$ in Eq. (2) can be used as an indication of the amount of sideband suppression. Infinite suppression occurs with X=1, so as $\Delta t/T$ increases the predicted sideband suppression decreases. This is what occurs for the actuator in the fiber stretcher. The flyback time Δt=0.5 ms (with ΔV=500 V) is fixed because of the maximum current available from high voltage amplifier. So, the actuator $\Delta t/T$ increases from 0.0125 to 0.025 and then to 0.050 at 25, 50, and 100 Hz respectively.

The second set of data, as shown in Fig. 15 (a-c), for the fiber-optic phase shift was taken with the same modulation frequencies as the other data sets. The difference is that the maximum phase shift is now 4π, m=2, which doubles the frequency translation $\Delta v=m/T=2/T$. The sideband spacing remains equal to the modulation frequency, so the frequency translated carrier now corresponds to sideband n=-2. To stretch the fiber by 4π at 12 GHz requires an actuator voltage of ~1000 V. The flyback time Δt is now 1.0 ms. The factor $\Delta t/T$ is twice the previous values, it is 0.025, 0.050, and 0.100 at 25, 50, and 100 Hz respectively. From this the sideband suppression is expected to be less than for the 2π stretching case; this is exactly what was observed. A summary of the sideband strengths of the frequency shifted spectrums at 12 GHz generated by serrodyne modulating the fiber optic and the general microwave model 7728 phase shifters (measured) are given in Table 2. The measured carrier suppression is >19, >16 and >13 dB at 25, 50, and 100 Hz respectively.

CONCLUSIONS

This report has compared the performance and characteristics of two phase shifters that use very different approaches. The General Microwave 7728, a conventional p-i-n diode phase shifter uses a very mature technology compared to the fiber-optic phase shifter, where the phase is varied by physically stretching the optical fiber. Each phase shifter is capable of generating a 2π shift at 6 GHz with devices of comparable size. The significant characteristic is that the optical fiber phase shifter produces a multi-octave true-time delay in contrast to the frequency independent phase shift of the p-i-n diode phase shifter. In addition, the fiber-optic phase shifter introduces a minimal amount of amplitude and phase variation over this multi-octave frequency range.

Table 1 outlines several comparison parameters of this report. The size, power consumption, weight, volume, and phase shifting capability show that the fiber-optic phase shifter is a practical option for a hybrid RF/fiber-optic system. It should be noted that there is flexibility in the form of the fiber-optic phase shifter. This particular configuration was chosen to avoid overlapping fibers and uses an off-the-shelf peizoelectric actuator. It is possible to package this phase shifter in different forms. Also, the fiber-optic phase shifter was designed to generate a one wavelength phase shift at 6 GHz. The phase shifter can be redesigned to produce several orders of magnitude of wavelength phase shift. This would require a proportional increase in fiber with a proportional increase in propagation delay.

The phase vs frequency and phase setting shows that the fiber-optic phase shifter performs with greater accuracy. The amplitude vs frequency and phase setting shows that the fiber-optic phase shifter produces a phase shift modulation independent of amplitude modulation. This is a desired characteristic.

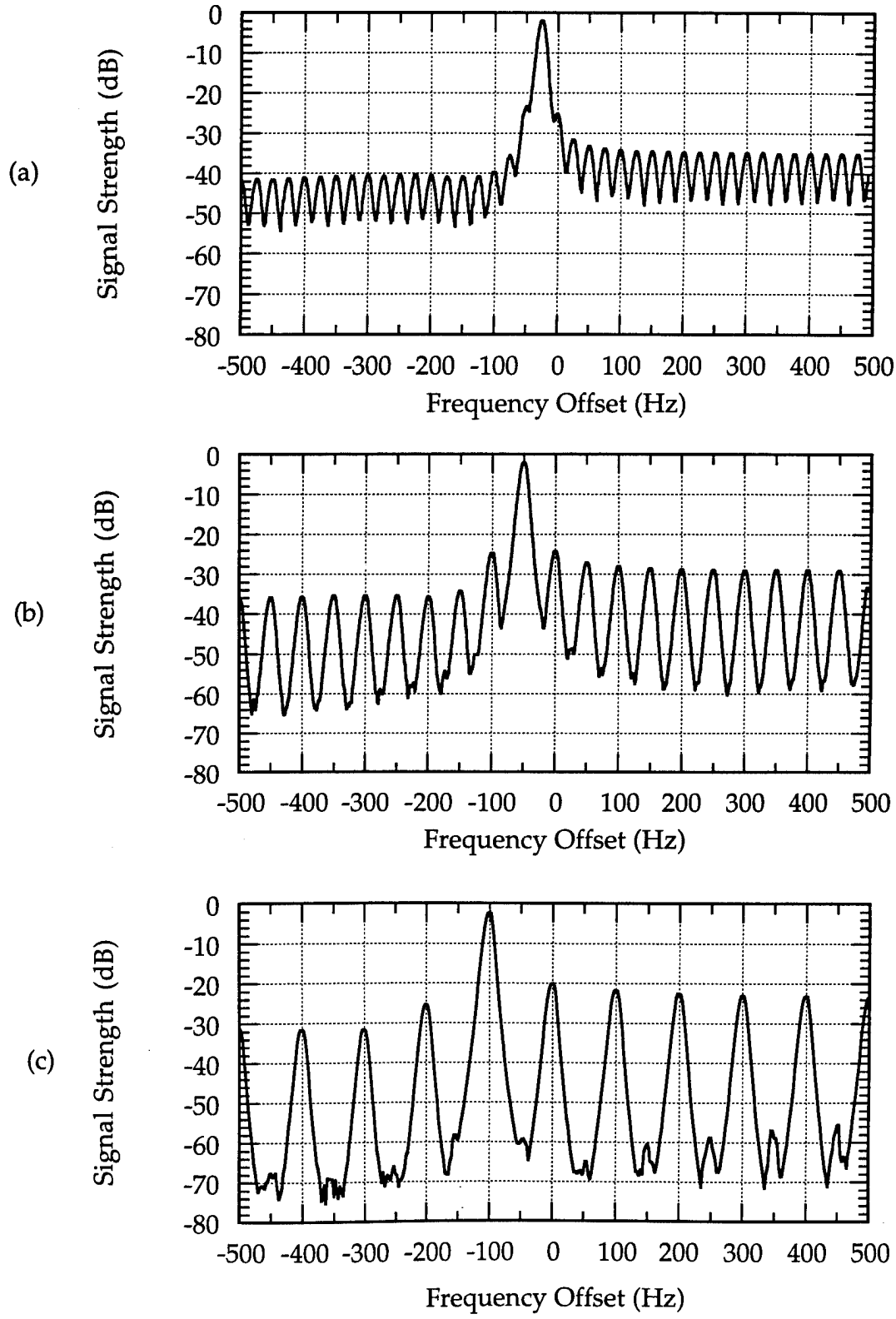

Fig. 14 — Microwave spectrum analyzer output demonstrating the frequency shift generated by the fiber-optic phase shifter at 12 GHz with a 2π serrodyne modulation at, (a) 25 Hz, (b) 50 Hz, and (c) 100 Hz (measured)

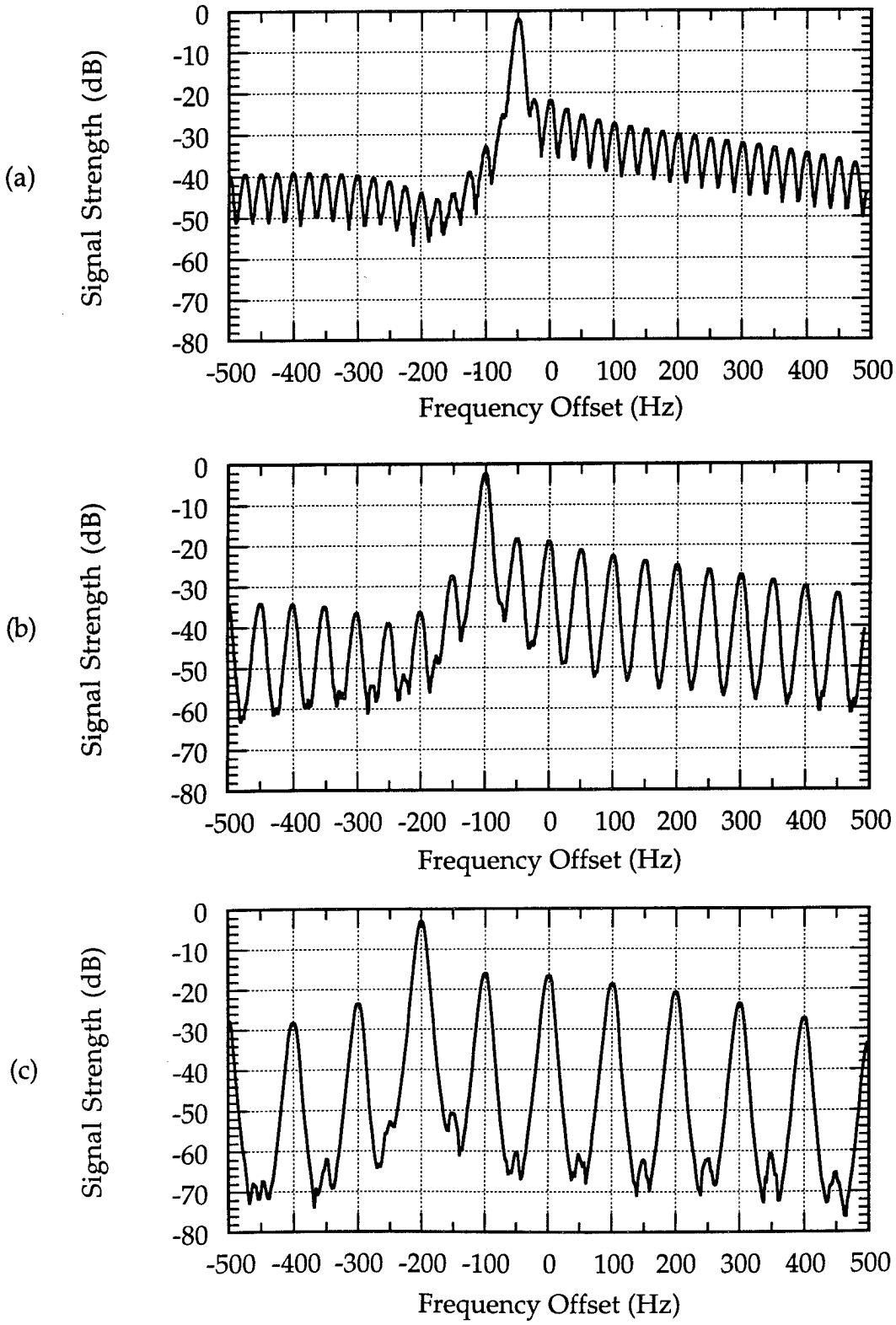

Fig. 15 — Microwave spectrum analyzer output demonstrating the frequency shift generated by the fiber-optic phase shifter at 12 GHz with a 4π serrodyne modulation at, (a) 25 Hz, (b) 50 Hz, and (c) 100 Hz (measured)

Table 2 — Summary of the Sideband Strengths

Modulation Frequency	Δø	Sibeband — Signal Strengths (dB)						
		-4	-3	-2	-1	0	1	2
Fiber Optic								
25 Hz	2 π			-21.7	-0.3	-23.5	-29.9	
50	2 π			-23.0	-0.3	-22.6	-25.5	
100	2 π			-27.1	-0.6	-18.5	-20.1	
Fiber Optic								
25 Hz	4 π	-31.4	-24.5	-0.4	-20.1	-20.3	-22.5	-27.3
50	4 π	-34.5	-25.8	-0.8	-16.8	-17.4	-20.0	-21.0
100	4 π	-26.7	-22.0	-1.4	-14.5	-14.7	-17.0	-19.1
P-I-N Diode								
	2 π			-29.1	-0.6	-28.2	-26.3	
25 Hz	2 π			-37.3	-0.7	-29.0	-26.3	
50	2 π			-37.0	-0.7	-29.0	-26.3	
100								

The sideband suppression for the fiber-optic phase shifter would be greatly improved if the flyback time Δt was decreased. This can be accomplished in one of two ways. First, the high voltage amplifier used in this study, with a peak current 0.5 A at 1000 V, could be replaced by one that can supply a larger current. The peak current could be increased, but the cost would be prohibitive if the increase is more than a factor of 5 or 10. This is because of the limitations in electronic components at this voltage level. The second approach to decrease Δt has more potential; new lower voltage configurations of the piezoelectric actuators are becoming commercially available [11]. A low voltage actuator with an expansion and pushing force similar to the actuator used in this study requires a maximum drive voltage of only 100 V. The drawback is that its capacitance is approximately an order of magnitude larger. From Eq. (6) the decrease in voltage is canceled out by the increase in capacitance, so approximately the same drive currents will be required for either type of actuator. However, at this lower voltage of 100 V it is much easier to generate the larger currents that are needed to significantly reduce Δt, and therefore increase the carrier and sideband suppression.

In summary the p-i-n diode and fiber-optic shifters have their respective advantages. The p-i-n diode currently exhibits faster switching speed, less power consumption, and less insertion delay.. The fiber-optic device exhibits wideband, true time-delay, lower loss, less amplitude variation, better phase accuracy, and can be easily integrated into existing fiber-optic systems. In a particular application, frequency translation, the initial tests revealed that the fiber-optic phase shifter needs to have its carrier and sideband suppression improved by 5 to 10 dB to match the p-i-n diode performance. This improvement could be achieved, as discussed in the theory section, by decreasing the actuators nonlinearity, hysteresis, and flyback time, which would result a more ideal serrodyne modulation of the phase. An actuator, using new piezoelectric material [15] and constructed by using the low voltage configuration, has the potential of producing a phase variation much closer to this ideal waveform.

ACKNOWLEDGMENTS

This work was funded through the Advanced Signals and LPI Countermeasures effect under the Office of Naval Research (ONR) 6.2 Electronic Warfare (EW) block. The authors wish to express their appreciation to Captain Kasuda for his continued support.

The authors also wish to thank Kieth J. Williams of the Optical Sciences Division at the Naval Research Laboratory for this work on the original fiber-optic phase shifter and his useful discussions in building the present version.

REFERENCES

1. M. Kam, J. Wilcox and P.R. Herczfeld, "Design for Steering Accuracy in Antenna Arrays Using Shared Optical Phase Shifters," *IEEE Trans. Antenna and Propagation*, **37**(9), 1102 (1989).

2. A. Krycuk, J. Fugitt, K. Mahoney and S. Simrock, "The CEBAF frequency distribution system," *IEEE Particle Accelerator Conference. Accelerator Science and Technology*, **3**, 1470 (1991).

3. G. Klein and L. Dubrowsky, "The DIGILATOR, a New Broadband Microwave Frequency Translator," *IEEE Trans. MTT*, **15**(3), 172 (1967).

4. R.C. Cumming, "The Serrodyne Frequency Translator," Proceedings of the IRE, 1957, V. 45, pp. 175.

5. L.B. Van Brunt, *Applied ECM*, Dunn Loring, VA: EW Engineering, Inc., 1978.

6. E. Voges, O. Ostwald, B. Schiek and A. Neyer, " Optical Phase and Amplitude Measurement by Single Sideband Homodyne Detection," *IEEE J. of Quantum Electronics*, **18**, 124 (1982).

7. L. Thylen, P. Sjoberg, and G.E. Lindqvist, "Electro-optical serrodyne frequency translator for λ=1.3 μm," IEE Proceedings, 1985, 132, pp. 119.

8. A. Ebberg and G. Schiffner, "Closed-loop fiber-optic gyroscope with a sawtooth phase-modulated feedback," *Optics Letters*, **10**, 300 (1985).

9. L.M. Johnson, C.H. Cox, "Serrodyne Optical Frequency Translation with High Sideband Suppression," *J. of Lightwave Technology*, **6**(1), 109 (1988).

10. C. Laskoskie, H. Hung, T. EL-Wailly, and C.L. Chang, "Ti-$LiNbO_3$ Waveguide Serrodyne Modulator with Ultrahigh Sideband Suppression for Fiber-Optic Gyroscopes," *J. of Lightwave Technology*, **7**(4), 600 (1989).

11. Physik Instrumente, *Products For Micropositioning*, p. 59.

12. E.H. Anderson, D.M. Moore, J.L. Fanson and M.A. Ealey, "Development of an active truss element for control of precision structures," *Optical Eng.*, **29**, 1333 (1990).

13. R.G. White and D.C. Emmony, "Active feedback stabilisation of a Michelson interferometer using a flexure element," *J. Phys.E: Sci. Instrum.*, **18**, 658 (1985).

14. M.G. Harris and D.M. Gibbs, "A Piezoelectric Actuated Scanning Mirror System Utilizing a Type One Control Loop," IEEE Proceedings - 1989 Southeastcon, pp. 1267.

15. N. Okada, K. Ishikawa, T. Nomura, K. Murakami, S. Fukuoka, N. Nishino, and U. Kihara, "Low-Hysteresis Actuator of Alkoxide-Prepared $Pb_{0.96}Sr_{0.04}(Zr_{0.51}Ti_{0.49})O_3$," *Japanese J. of Applied Physics*, **30**, 2267 (1991).

16. G.S. Glaesemann and S.T. Gulati, "Design methodology for the mechanical reliability of optical fiber," *Optical Eng.*, **30**, 709 (1991).

17. N. Lagakos, J.A. Bucaro, and R. Hughes, "Acoustic sensitivity predictions of single-mode optical fibers using Brillouin Scattering," *Applied Optics*, **19**, 3668 (1980).

18. T. Kokubun, Y. Katsuyama, K. Hogari, and S. Hatano, "Resin Selection and High-Speed Coating of Optical Fibers with UV-Curable Materials," *J. of Lightwave Technology*, **7**(5), 824 (1989).

19. J.J. Carr, S.L. Saikkonen, and D.H. Williams, "Refractive Index Measurements on Single-Mode Fiber as Functions of Product Parameters, Tensile Stress and Temperature," *Fiber and Integrated Optics*, **9**, 393 (1990).